



Research Paper

Mitochondrial oxidative stress in the retinal pigment epithelium (RPE) led to metabolic dysfunction in both the RPE and retinal photoreceptors



Emily E. Brown^{a,b}, Alexander J. DeWeerd^a, Cristhian J. Ildefonso^a, Alfred S. Lewin^c, John D. Ash^{a,*}

^a Department of Ophthalmology, College of Medicine, University of Florida, Gainesville, FL, USA

^b Clinical and Translational Science Institute, University of Florida, Gainesville, FL, USA

^c Department of Molecular Genetics and Microbiology, College of Medicine, University of Florida, Gainesville, FL, USA

ARTICLE INFO

Keywords:

Retina
SOD2
AMD
Mitochondria

ABSTRACT

Age-related macular degeneration (AMD) is the leading cause of vision loss in the western world. Recent evidence suggests that RPE and photoreceptors have an interconnected metabolism and that mitochondrial damage in RPE is a trigger for degeneration in both RPE and photoreceptors in AMD. To test this hypothesis, this study was designed to induce mitochondrial damage in RPE in mice to determine whether this is sufficient to cause RPE and photoreceptor damage characteristic of AMD. In this study, we conditionally deleted the gene encoding the mitochondrial antioxidant enzyme, manganese superoxide dismutase (MnSOD encoded by *Sod2*) in the retinal pigment epithelium (RPE) of albino BALB/cJ mice. *VMD2-Cre;Sod2^{flax/flax}* BALB/cJ mice were housed in either 12-h dark, 12-h 200 lux white lighting (normal light), or 12-h dark, 12-h < 10 lux red lighting (dim light). Electroretinography (ERG) and spectral-domain optical coherence tomography (SD-OCT) were performed to assess retinal function and morphology. Immunofluorescence was used to examine protein expression; quantitative RT-PCR was used to measure gene expression. *Sod2* knockout (KO) mice had reduced RPE function with age and increased oxidative stress compared to wild type (WT) controls as expected by the cell-specific deletion of *Sod2*. This was associated with alterations in RPE morphology and the structure and function of RPE mitochondria. In addition, data show a compensatory increase in RPE glycolytic metabolism. The metabolic shift in RPE correlated with severe disruption of photoreceptor mitochondria including a reduction in TOMM20 expression, mitochondrial fragmentation, and reduced COXIII/ β -actin levels. These findings demonstrate that mitochondrial oxidative stress can lead to RPE dysfunction and metabolic reprogramming of RPE. Secondary to these changes, photoreceptors also undergo metabolic stress with increased mitochondrial damage. These data are consistent with the hypothesis of a linked metabolism between RPE and photoreceptors and suggest a mechanism of retinal degeneration in dry AMD.

1. Introduction

Mitochondrial dysfunction has been associated with general aging, as well as a variety of age-related diseases, such as Alzheimer's disease and Parkinson's disease [1–4]. Recent evidence suggests that mitochondrial damage and oxidative stress in the retinal pigment epithelium (RPE) may play an important role in disease pathogenesis in age-related macular degeneration (AMD) [5,6]. AMD is the leading cause of blindness in older individuals in industrialized countries [7]. AMD results in a loss of central vision, leading to a major decrease in quality of life. Although there are therapies available to treat one form of late stage AMD, known as neovascular AMD [8–10], there are

currently no FDA-approved therapies or treatments for early AMD or the other late stage AMD, known as geographic atrophy.

AMD is a multifactorial disorder affecting many cell types in the retina including choriocapillary endothelial cells, microglia, photoreceptors, and RPE [11]. The RPE are responsible for maintaining the blood-retina barrier, providing the retina with nutrients from the blood supply, phagocytosing the photoreceptor outer segments, recycling the visual chromophore for the visual cycle, and absorbing excess light to prevent photo-oxidation. Without proper RPE function, the photoreceptors cannot survive, thus leading to subsequent vision loss.

AMD has been associated with alterations in mitochondria in the RPE, including disrupted mitochondrial morphology, increases in

* Corresponding author. University of Florida, 1600 SW Archer Road Gainesville, FL, 32610, USA.

E-mail address: jash@ufl.edu (J.D. Ash).

<https://doi.org/10.1016/j.redox.2019.101201>

Received 22 March 2019; Received in revised form 10 April 2019; Accepted 11 April 2019

Available online 20 April 2019

2213-2317/ © 2019 The Authors. Published by Elsevier B.V. This is an open access article under the CC BY-NC-ND license (<http://creativecommons.org/licenses/by-nc-nd/4.0/>).

mitochondrial DNA lesions, and mitochondrial dysfunction [5,6,12,13]. Dry AMD is characterized by loss of RPE function and a subsequent loss of rod photoreceptors. The mechanism for this linked degeneration is poorly understood. Recent evidence suggests that the metabolism in the retina is highly coordinated in a metabolic ecosystem [14]. Particularly, the interaction of metabolism between the photoreceptors and RPE is essential for proper function of both cell types. The RPE are responsible for transporting glucose from the choroid to the photoreceptors. Increasing lactate concentration in cultured RPE cells has been reported to reduce glucose utilization by the RPE [14]. The authors suggested that lactate may be the signal that inhibits the RPE from utilizing glucose, thus allowing its transport to photoreceptors. Photoreceptors utilize glucose for aerobic glycolysis and produce large amounts of lactate even in the presence of oxygen. This lactate is then transported to the RPE cells, which use it for energy production through oxidative phosphorylation. Based on the metabolic ecosystem model, we hypothesize that elevated mitochondrial dysfunction in the RPE will result in RPE switching to glycolysis, which is anticipated to reduce glucose availability to photoreceptors leading to potential energy crisis and photoreceptor dysfunction.

In order to test the hypothesis that mitochondrial damage in the RPE contributes to RPE dysfunction, secondary photoreceptor degeneration, and progression of AMD, we used RPE-specific *Cre* expression to delete the gene encoding the mitochondrial antioxidant enzyme, MnSOD specifically in RPE. We aimed to determine how increased mitochondrial damage and oxidative stress in RPE would affect function, metabolism, and survival of both RPE and rod photoreceptors. We used non-invasive *in vivo* assays to assess retinal function and morphology, to test our hypothesis that increased mitochondrial oxidative stress in the RPE results in RPE dysfunction and that this dysfunction will lead to secondary effects on photoreceptors. Our results show major differences in retinal function and mitochondrial morphology when comparing *Sod2* knockout (KO) and wild type (WT) mice, an increase in glycolytic gene expression in the RPE, and secondary effects on photoreceptors.

2. Methods

2.1. Animals

Mice with conditional knockout of *Sod2* in the RPE in a C57BL/6J background (*VMD2-Cre;Sod2^{flox/flox}* C57BL/6J mice) [15] that carry the human RPE-specific gene promoter, *VMD2*, driving the tetracycline-inducible transactivator gene (rtTA) were utilized [16]. These mice contain *loxP* sites that flank exon 3 of the *Sod2* gene [17] resulting in a doxycycline-inducible RPE-specific deletion of *Sod2*.

VMD2-Cre;Sod2^{flox/flox} C57BL/6J mice were backcrossed to BALB/cJ mice for a minimum of six generations. Genotyping was performed on tail or ear biopsy samples for *Cre*, as described by Le et al. [16], for *Sod2*, as described by Strassburger et al. [17], for Nicotinamide Nucleotide Transhydrogenase (NNT) as described by Ronchi et al. [18], and for the absence of common mutations causing retinal degeneration [19–21]. Mice were confirmed to be wild type for mutations associated with retinal degenerations and for NNT. *VMD2-Cre;Sod2^{flox/flox}* mice heterozygous for *Cre* were bred to *Cre*-negative *Sod2^{flox/flox}* mice. *Cre* expression was induced by feeding chow containing 200 mg/kg doxycycline to nursing dams (Bioserv, S3888). Upon wean, pups were given doxycycline chow for 15 days, and then given normal rodent diet for the remainder of their lives. Importantly, mice were off doxycycline-containing chow for several weeks before their first analysis. *VMD2-Cre* mice with no alleles with *loxP* sites were used to assess levels of *Cre* toxicity.

Both male and female *VMD2-Cre;Sod2^{flox/flox}* BALB/cJ or *VMD2-Cre* mice were reared in 12-h dark, 12-hour < 150 lux red light (lights on at 6 a.m.) from birth until wean. Upon wean, mice were either housed in 12-h dark, 12-hour 200 lux white lighting (normal light), or 12-h

dark, 12-h < 10 lux lighting (dim light) (lights on at 6 a.m. for both conditions). Food and water were given *ad libitum*. All procedures are conducted on male and female mice according to the ARVO Statement for Use of Animals in Ophthalmic and Vision Research and the National Institutes of Health Guide for the Care and Use of Laboratory animals (NIH Publications No. 8023, revised 1978) and were approved by the University of Florida Institutional Animal Care and Use Committee.

2.2. Spectral-domain optical coherence tomography

SD-OCT analysis of mice was performed as previously described [22].

2.3. Electroretinography

Electroretinography was performed as described [22] with the following deviations. Light stimulations using a xenon light source were carried out at the following intensities and adaptation times: 0.1 (P) cd.s/m² flash, 30 s adaptation, 1 (P)cd.s/m² flash, 30 s adaptation, 10 (P)cd.s/m² flash, 120 s adaptation, 100 (P)cd.s/m² flash, 120 s adaptation, and a final 200 (P)cd.s/m² flash.

2.4. Immunohistochemistry

Immunohistochemistry was performed as previously described [22]. Primary antibodies or stains, the manufacturers, catalog numbers, and dilutions used are as follows: TOMM20 (Abcam, ab186734, 1:200), SOD2 (Millipore, 06-984, 1:200), SOD2 (Millipore, MAB4081, Mouse, 1:400), 8OHdG (Abcam, ab26842, Mouse, 1:200), phalloidin (Alexa Fluor 488 Phalloidin, Molecular Probes, A12379, diluted according to manufacturer's instructions), and DAPI (Vector Laboratory, Burlingame, CA, 1:7500). Secondary antibodies used were conjugated to AlexaFluor 488 and AlexaFluor 594 (Thermo Fisher).

2.5. Microscopy

For fluorescence microscopy, the Keyence BZ-9000 and the Leica DMi8 inverted microscope were used to take images at 40X and 60X magnifications.

2.6. RNA isolation and qRT-PCR

For RNA: The RPE/choroid complex or neuroretina was dissected out and placed in Trizol reagent (Invitrogen, 15596026) and RNA was extracted according to the manufacturer's protocol. To obtain cDNA templates, iScript reverse transcription mix was used (Bio-Rad; Hercules, CA). *For Real-Time PCR:* Primers were designed as described [22]. Real-time PCR was performed using Ssofast SYBR Green Supermix (Bio-Rad; Hercules, CA) and the MyiQ Single-Color Real-Time PCR system (Bio-Rad; Hercules, CA) using the manufacturer's instructions and as described [22]. Primer sequences are listed in [Supplementary Table 1](#). Primers for PKM1 and PKM2 were obtained from Casson et al. [23]. mRNA expression was normalized to RPL19 and then to the WT control.

2.7. Determining mitochondrial DNA copy number

The RPE/choroid complex or neuroretina was isolated and digested in digestion buffer (100 mM EDTA, pH = 8.0, 50 mM Tris HCl, pH = 8.0, 0.5% SDS in H₂O, and 20 mg/mL proteinase K) overnight. Genomic DNA was extracted using phenol: chloroform: isoamyl alcohol, DNA was diluted to a final concentration of 50–100 ng/μl, and real-time PCR was performed as described above. Primer sequences are listed in [Supplementary Table 1](#).

2.8. Measuring ATP content

ATP in the RPE/choroid complex or neuroretina was measured using a fluorometric ATP Assay Kit, according to the manufacturer's protocol (ab83355, Abcam; Cambridge, Massachusetts). In brief, retinas or RPE/choroid complexes were dissected and pooled (neuroretinas or RPE/choroid complexes of 2 mice were pooled in each sample) and flash frozen in liquid nitrogen. After all eyes were dissected, tissue was thawed and homogenized in 25 μ L assay buffer using a 2 mL Dounce homogenizer. Next, the sample was centrifuged at 13,000 g for 5 min at 4 °C. The supernatant was collected and kept on ice. The sample, or known standards, were combined with the ATP reaction mix or background control mix in duplicates and incubated at room temperature for 30 min. The output was measured on a microplate reader at OD 570 nm. Calculations were performed according to the manufacturer's directions and values were normalized to WT.

2.9. Electron microscopy

Mice were euthanized using cervical dislocation. Eyes were carefully enucleated and placed in freshly made 2.5% glutaraldehyde in 0.1 M phosphate buffer (pH 7.4) fixative and dissected. Tissue preparation and imaging were performed as described previously [24].

2.10. Image quantifications

RPE cell area was quantified from three areas near the optic nerve and three areas in the periphery, maintaining consistency among the samples. RPE cell area and mitochondrial width, length, and cross-sectional area were quantified manually utilizing the ImageJ Software (NIH) measurement function [25]. For quantification of Sod2-positive RPE cells, phalloidin staining was utilized to determine the total number of cells. For quantification of 8-OHdG-positive nuclei the number of nuclei positive for 8-OHdG was divided by the total number of nuclei for each sample and these values were averaged for each group.

2.11. Statistical analysis

GraphPad Prism (La Jolla, CA) was used for analysis of statistics. Paired or unpaired t-tests were used to assess differences among two groups. Differences among more than two groups were assessed using analysis of variance (ANOVA) with a Tukey post-hoc test. Differences among males and females in each group were assessed using these methods, and no differences were found between genders. P-values equal to or less than 0.05 were considered statistically significant.

3. Results

3.1. Deletion of Sod2 in the RPE with increased susceptibility to photo-oxidative stress

Previous studies in C57BL/6J mice showed that deletion of Sod2 in the RPE results in an age-related decline in photoreceptor and inner retinal function and thickness of the layer of the retina containing the photoreceptor nuclei (known as the outer nuclear layer, ONL) [15]. To better understand the role of elevated mitochondrial oxidative stress in the RPE, we bred mice with an RPE-specific Cre (*VMD2-Cre*) on a BALB/cJ background. Cre-positive *Sod2^{fllox/fllox}* mice will be referred to as KO and Cre-negative *Sod2^{fllox/fllox}* mice, will be referred to as WT.

We chose to use a BALB/cJ background because these mice do not produce melanin, which increases their susceptibility to photo-oxidative stress. Additionally, unlike C57BL/6J mice, BALB/cJ mice express the same fully active variant of a protein involved in recycling of the visual chromophore, RPE65, as humans. These differences allow us to test whether environmental stressors, such as increased light exposure,

could affect RPE function. Additionally, C57BL/6J mice harbor a loss of function mutation in the gene encoding nicotinamide nucleotide transhydrogenase (Nnt) [26], an enzyme that plays an important role in regulation of oxidative stress [27–29]. Other genetic factors that may affect levels of oxidative stress include a deletion in the gene encoding the supercomplex assembly factor 1 (Scaf1), which has been associated with decreased oxidative stress [30]. However, this deletion is present in both C57BL/6J and BALB/cJ mice [31].

As been reported previously in the C57BL/6J mice, we found similar efficiency of Sod2 deletion in the RPE. We used RPE flat mounts to examine MnSOD expression using immunohistochemistry (IHC) in RPE from WT and KO mice (Supplemental Fig. 1A). Quantification showed that Sod2 expression remained in 14% of the RPE cells in the KO mice, but in 100% of the cells in the WT (Supplemental Fig. 1B).

3.2. Deletion of Sod2 results in reduced RPE function under conditions of increased photo-oxidative stress

Previous studies have not examined the effect of Sod2 deletion in the RPE on RPE function itself. To do this, we used electroretinography, a technique that measures retinal function in response to varying light stimuli, to measure retinal function in the mice as a function of age. Each component of the ERG corresponds to a different group of cells in the retina. The negative deflection, a-wave, corresponds to the photoreceptors hyperpolarizing in response to light. The positive wave-form, b-wave, is measured from the base of the negative a-wave to the peak of the b-wave and corresponds to activity of the inner retina. The slower longer final wave form, the c-wave, corresponds to sum of signals consisting of a larger positive deflection from the RPE and a smaller negative deflection from the retinal glial cells [32]. Since the Sod2 deletion occurs in RPE cells and not in glial cells, the reduction in c-wave reflects reduced RPE function.

Other studies have also not examined the effects of photo-oxidative stress due to increased light exposure. Thus, we kept mice housed in either dim light, 10 lux light intensity in the cage, or in normal lighting, 200 lux in the cage, for the duration of their lives after wean. When we measured the c-wave, we found that mice kept in 10 lux lighting conditions had no differences in RPE function with age (Fig. 1A, Supplemental Fig. 2A). However, when mice were kept in 200 lux lighting, we found a reduction in ERG c-wave peak in KO mice as compared to WT mice by 5 months of age (Fig. 1B, Supplemental Fig. 2A). This reduction in the c-wave peak was at the median ERG stimulation light intensity (Supplemental Fig. 2B). Inner retina and photoreceptor function were not different between KO and WT in normal or dim lighting at any age examined (Supplemental Figs. 2C and D).

Although doxycycline-induced Cre is only expressed from embryonic day nine to postnatal day 60, with peak induction at postnatal day four [16], we wanted to confirm that differences in RPE function were not due to toxicity to Cre itself. To do this, we used *VMD2-Cre* mice lacking loxP sites. We found no differences between *VMD2-Cre*-positive and *VMD2-Cre*-negative a-wave, b-wave, and c-wave amplitudes at 5 months of age (Supplemental Figs. 3A and B). These findings are consistent with the findings of Le et al. who developed the initial *VMD2-Cre* mice for inducible RPE-specific Cre expression [16].

Since we observed a loss of RPE function at 5 months of age in *VMD2-Cre;Sod2^{fllox/fllox}* mice, we wanted to see if this reduction in function corresponded with any alterations in retinal morphology. Previous studies in C57BL/6J mice found reduced ONL thickness with aging, by 6–9 months of age [15]. Using spectral-domain optical coherence tomography (SD-OCT), a non-invasive method to examine retinal morphology *in vivo*, we are able to visualize the different layers of the retina. The ONL, which contains the photoreceptor nuclei, represents the photoreceptor viability as this layer thins with photoreceptor cell death. We saw no gross morphological changes in retina structure by SD-OCT in mice kept at normal lighting (Fig. 1C) or dim

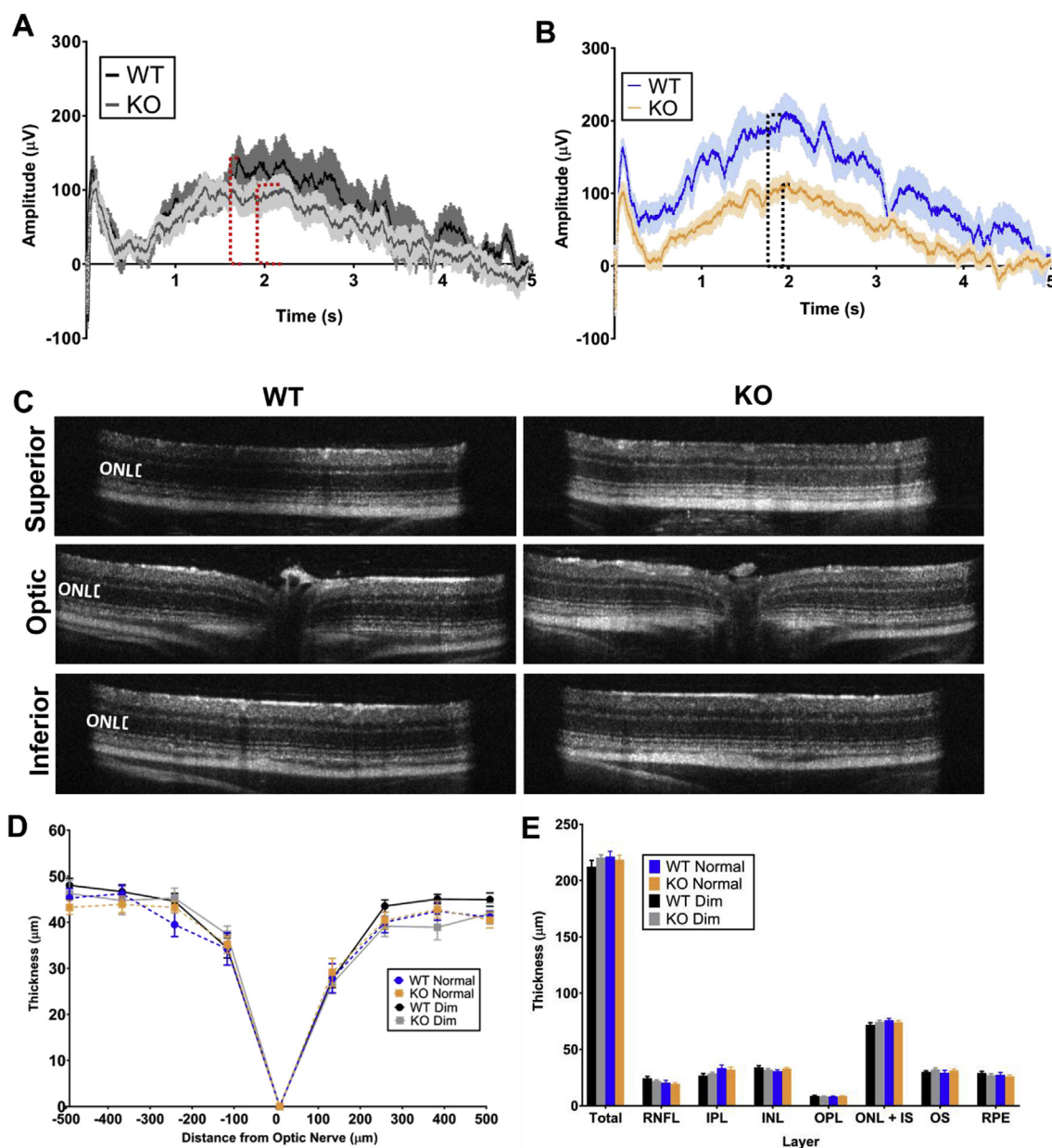


Fig. 1. Deletion of *Sod2* results in light-dependent loss of RPE function. **A-B**) ERG trace at 1 log (P)cd.s/m² at 5 months of age in dim lighting (**A**) and normal lighting (**B**), $n \geq 9$. Dashed lines indicate c-wave amplitude. **C**) Representative OCT images of superior (300 μm from optic nerve), optic nerve, and inferior (-300 μm from optic nerve) in wild type and knockout at 5 months of age in normal lighting. **D**) Quantification of outer nuclear layer (ONL) thicknesses at various distances from optic nerve at 5 months of age in normal lighting or dim lighting. Two-way ANOVA, $P \geq 0.86$, $n \geq 5$, plotted error = SEM. **E**) Average thicknesses of various retinal layers at 5 months of age in normal lighting or dim lighting. Two-way ANOVA, $P \geq 0.30$, $n \geq 5$, plotted error = SEM.

lighting (not shown) by 5 months of age. We found no measurable differences in thickness of ONL or any other layers in mice kept in dim or normal lighting by 5 months of age (Fig. 1D and E). There were also no differences in thicknesses at 1–4 months of age (not shown). Additionally, no changes in retinal morphology were observed in *VMD2-Cre* control mice (Supplemental Figs. 3C–D).

3.3. Deletion of *Sod2* disrupts RPE cell morphology and leads to alterations in mitochondrial distribution and morphology

Although we did not observe gross morphological differences in the whole retina by SD-OCT, RPE morphology cannot be investigated in detail by this technique. As we observed initial loss of RPE function in KO mice at 5 months of age in mice kept in normal lighting, we collected RPE flat mounts at this age to examine RPE cell morphology

using phalloidin to label the F-actin cytoskeleton present at RPE cell boundaries. Previous studies have not measured RPE cell area to assess RPE morphology with loss of *Sod2*. We assessed the area of each RPE cell in the central retina or peripheral retina (Fig. 2A). Quantification of the average RPE cell area in the central retina shows that the KO mice had increased cell area as compared to the WT (Fig. 2B). The difference in cell area between the KO and WT in the peripheral region did not reach statistical significance (Fig. 2B).

As previous studies did not assess mitochondria in the RPE, we assessed how loss of MnSOD might affect mitochondrial morphology in the RPE. To do this, we used an antibody against the translocase of the outer mitochondrial membrane 20 (TOMM20) on RPE flat mounts. We decided to focus on mice kept in 200 lux, normal lighting, at 5 months of age because this is where we observe a reduction in RPE function. In the WT, TOMM20 staining was uniformly spread within RPE cells, and

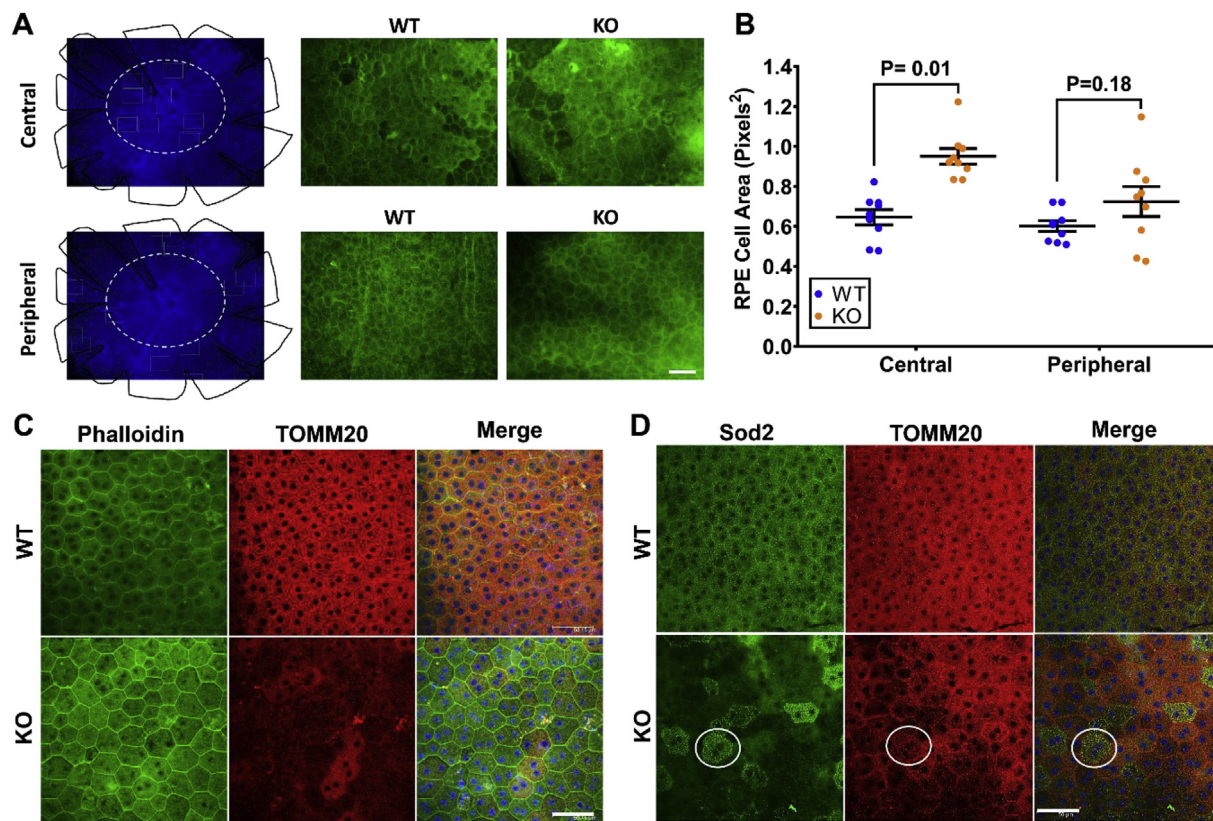


Fig. 2. Alterations in mitochondrial localization and RPE morphology with deletion of *Sod2*. **A**) Merged images of all RPE flat mounts (blue represents DAPI staining, black lines represent general area of flat mounts). Area inside the white dotted ellipse represents the central region, near the optic nerve (top), while the area outside the white dotted ellipse represents the peripheral region (bottom). Representative images for the central areas (top right) and peripheral areas (bottom right) in the WT and KO using phalloidin (green). White line indicates scale bar = 50 μm . **B**) Quantification of average area per RPE cell (in pixels) from **A**. Unpaired *t*-test, $P = 0.01$ for central and $P = 0.18$ for peripheral, error bars represent SEM, $n = 3$ mice per group, 3 images in the central area and 3 images in the peripheral area per eye. Dots represent average RPE cell area per image. **C**) Representative IHC images of RPE flat mounts from 5-month-old *Sod2* WT (top panel) or KO (bottom panel) mice kept in normal lighting. Phalloidin (green) labels F-actin, TOMM20 (red) labels the mitochondrial outer membrane, and DAPI (blue) labels cell nuclei. Scale bar = 50 μm . **D**) Representative RPE flat mounts from 5-month-old *Sod2* WT (top panel) or KO (bottom panel) mice kept in normal lighting stained with markers for *Sod2* (green), TOMM20 (red), and DAPI (blue). Circle indicates a cell retaining *Sod2* expression but deficient in TOMM20. Scale bar = 50 μm .

labeling was consistent among all cells (Fig. 2C). However, in the knockout, there was a visible reduction in TOMM20, with lack of uniform staining (Fig. 2C). As there was not 100% deletion of *Sod2* in the RPE using the *Cre-loxP* system, we wanted to determine specifically how the cells without *Sod2* were affected. To do this, we co-stained RPE flat mounts with antibodies against MnSOD and TOMM20. Although we again observed the lack of uniformity of TOMM20 staining in the KO, the effect was not exclusive to the cells with *Sod2* deletion, suggesting that deletion of *Sod2* in some RPE cells may have a secondary effect on neighboring RPE cells, even in the presence of MnSOD (Fig. 2D).

3.4. Deletion of *Sod2* leads to mitochondrial swelling, reduced ATP content, and reduced COXIII/ β -actin levels

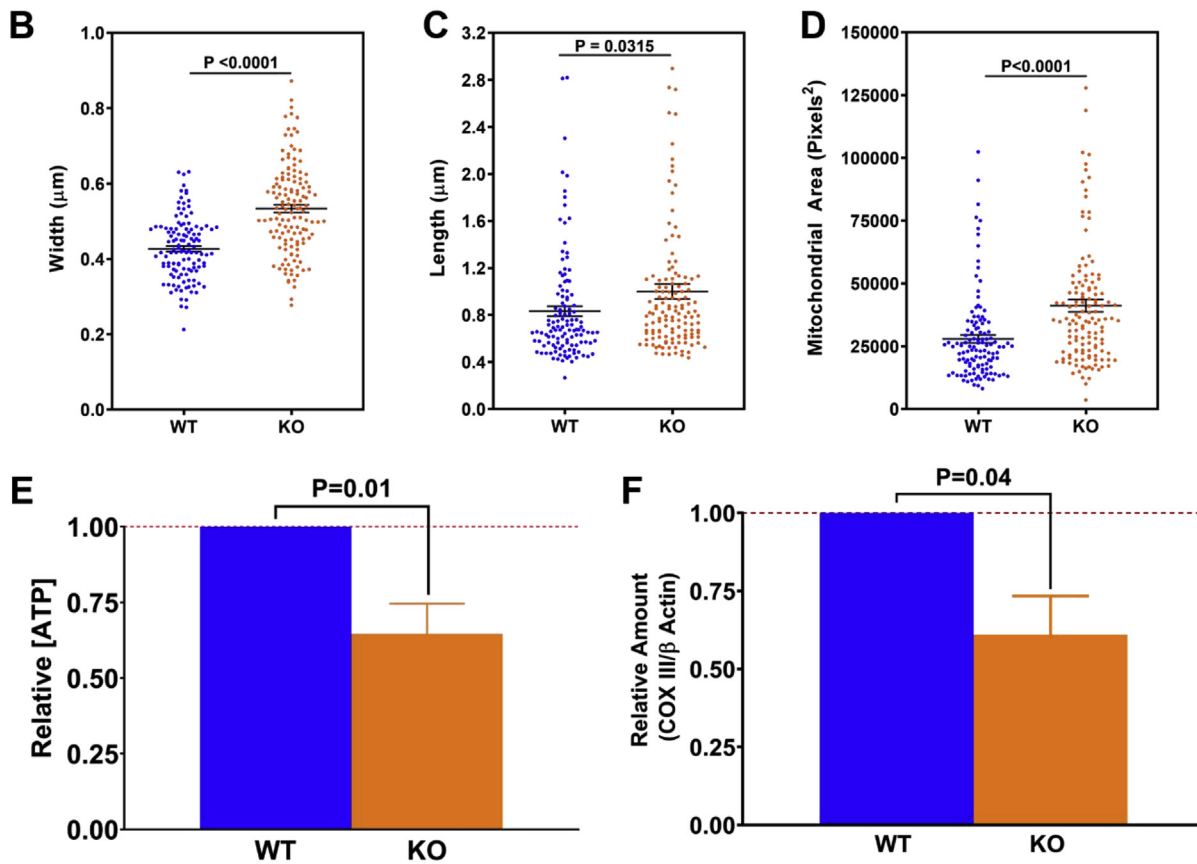
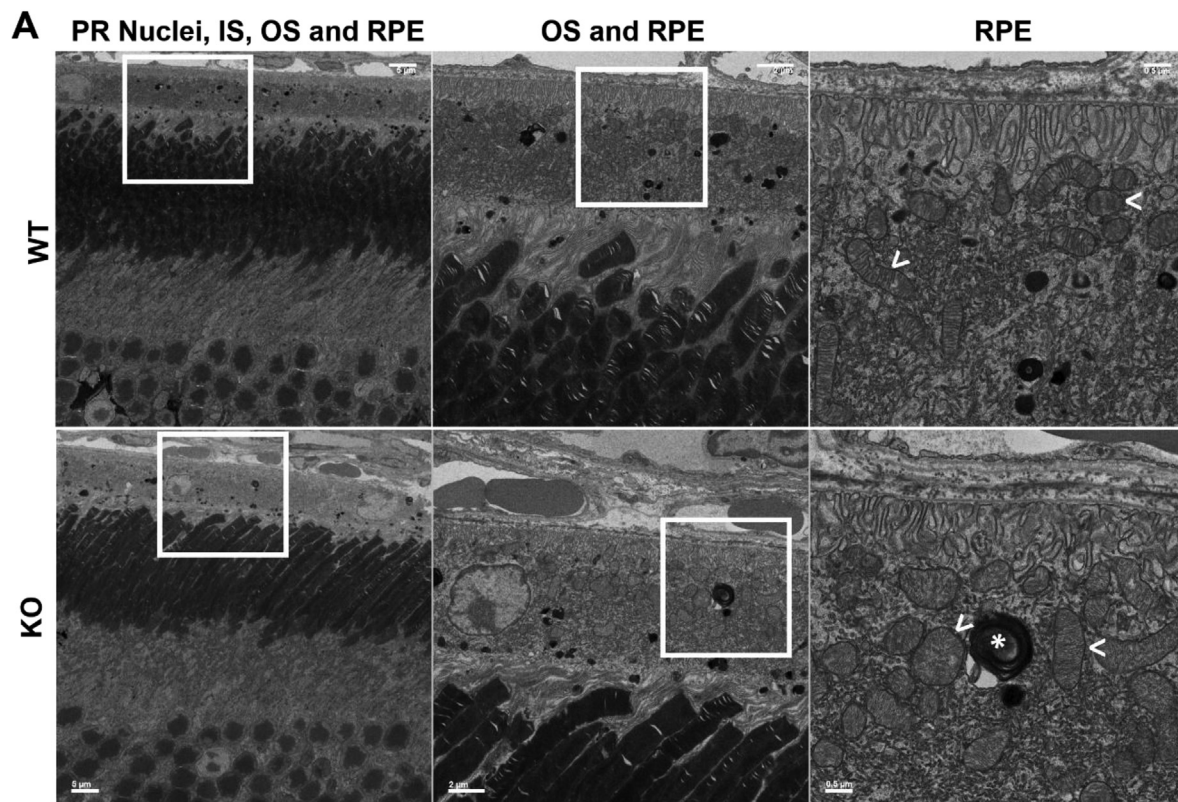
Since we observed alterations in mitochondrial staining and localization by IHC with *Sod2* KO, we wanted to examine how mitochondrial ultrastructural morphology may be altered. We used electron microscopy (EM) to assess mitochondrial morphology in the RPE in retinal cross sections. The mitochondria within the RPE of the WT mice were electron dense, with clearly organized cristae structure (Fig. 3A). In contrast, the mitochondria of the KO RPE were typically less electron dense and exhibited disorganized cristae. The mitochondria in the RPE cells of KO mice also appeared more swollen in comparison to those in the WT (Fig. 3A, bottom panel), and when we quantified the average mitochondrial width, length, and cross-sectional area, the KO mice had an increase in all three dimensions indicating distension of

mitochondria relative the WT (Fig. 3B–D).

Since we observed swelling of mitochondria in the RPE and disruption of cristae organization, we assessed how ATP production was affected. Previous studies did not examine how ATP and levels of mtDNA are impacted with knockout of *Sod2* in the RPE. Relative to ATP levels in the RPE in WT mice, the *Sod2* KO had a reduction in ATP in the RPE/choroid complex (Fig. 3E). To determine if removal of the protective enzyme was associated with alterations in mitochondrial DNA (mtDNA) levels, we measured DNA levels of mitochondrial-encoded cytochrome c oxidase subunit III (COX-III) in the RPE/choroid complex compared to levels of a nuclear-encoded gene, β -actin. Relative to the WT, *Sod2* KO RPE had a reduction in COXIII/ β -actin levels (Fig. 3F).

3.5. Deletion of SOD2 leads to elevated oxidative stress in the RPE

Because superoxide dismutase protects mitochondrial components from superoxide radicals generated as byproducts of mitochondrial electron transport, we investigated whether RPE cells lacking MnSOD were subject to increased oxidative stress. To investigate mitochondrial DNA damage, we stained retinal cross sections with an antibody for 8-hydroxy-2'-deoxyguanosine (8-OHdG), a marker of oxidative DNA damage due to oxidized deoxyguanosine. This damage can occur in both nuclear and mitochondrial DNA. We found elevated levels of 8-OHdG in the RPE in KO mice, as seen in the representative IHC images (Fig. 4A). The average percentage of 8-OHdG-positive RPE nuclei is shown in Fig. 4B. There was also staining in the KO, but not in the WT in the



(caption on next page)

Fig. 3. Mitochondrial alterations in the RPE with deletion of *Sod2*. A) Representative EM images from WT (top panel) and KO (bottom panel) 5-month-old mice kept in normal lighting. Column 1: RPE and photoreceptor outer segments, inner segments, and nuclear layer. Scale bar = 5 μ m. Column 2: RPE and photoreceptor outer segments. Scale bar = 2 μ m. Column 3: RPE. Scale bar = 0.5 μ m. Boxes indicate area magnified in following panel. < indicates mitochondria, * indicates electron dense material. For quantifications in B-D the highest magnification images with 0.5 μ m scale were used. B) Quantitation of average mitochondrial width. Dots represent individual mitochondria width. Unpaired *t*-test, $P < 0.0001$, $n = 3$ mice per group, 5 images per mouse. C) Measurement of average mitochondrial length. Dots represent length of individual mitochondria. Unpaired *t*-test, $P = 0.0315$, $n = 3$ mice per group, 5 images per mouse. D) Quantitation of average mitochondrial cross-sectional area. Dots represent cross sectional area of individual mitochondria. Unpaired *t*-test, $P < 0.0001$, $n = 3$ mice per group, 5 images per mouse. E) Relative ATP levels in the RPE in 5-month-old mice kept in normal lighting. Unpaired *t*-test, $P = 0.01$, $n = 5$ per group. F) Relative COXIII/ β -actin levels in RPE in 5-month-old mice kept in normal lighting. Unpaired *t*-test, $P = 0.04$, $n = 3$ WT and 4 KO. Plotted error = SEM for all graphs.

inner segments, where the mitochondria are most abundant within the photoreceptor cells. This staining co-localized with TOMM20 staining, suggesting that the mitochondria of the photoreceptor inner segments have increased oxidative DNA damage. Interestingly, the TOMM20 staining in the inner segments was reduced in the KO, as compared to the WT, suggesting that there may be alterations in the mitochondria in the photoreceptors as a secondary effect of increased RPE oxidative stress and reduced RPE function.

To assess oxidative stress by an independent technique, we used qRT-PCR to measure gene expression of several genes. We found increased expression of nuclear respiratory factor 1 (Nrf1), a transcription factor involved in regulation of mitochondrial DNA transcription and replication and cellular growth (Fig. 4C). We also observed increased expression of nuclear factor erythroid 2-related factor 2 (Nrf2), which is a transcription factor that regulates an oxidative stress response and metabolism (Fig. 4D).

3.6. Compensatory mechanisms in the RPE

We next wanted to determine whether there was upregulation of any compensatory mechanisms in the RPE, such as increased mitochondrial transcription or enhanced glycolysis due to disruption of mitochondria. To this end we measured gene expression of mitochondrial-related and glycolysis-related genes in the RPE/choroid complex.

We detected elevated levels of transcription factor A (TFAM), involved in mitochondrial transcription and mtDNA replication (Fig. 5A) in the KO mice at 5 months of age in the normal lighting, as compared to the WT. This may reflect a compensatory mechanism, since we also detected a reduction in mitochondrial DNA content in KO mice. Other studies have found increased TFAM expression in aging [33] and in hybrid cells containing mitochondrial mutations [34].

To assess whether there were increases in glycolysis as a result of a reduction in mitochondrial health, we investigated gene expression levels of key glycolysis-related genes in the RPE/choroid complex. We measured expression of hexokinase 1, which is responsible catalyzing the first step of glycolysis, converting glucose to glucose-6-phosphate, utilizing ATP. We found an increase in hexokinase expression in the KO as compared to the WT (Fig. 5B). We also measured expression of phosphofructokinase 1 (PFK1), which is responsible for catalyzing the phosphorylation of fructose-6-phosphate to fructose-1,6-bisphosphate, utilizing ATP. We found an increase in PFK1 expression in the KO as compared to the WT (Fig. 5C). We also measured expression of pyruvate kinases (PK) isoforms M1 (PKM1) and M2 (PKM2). Pyruvate kinase is responsible for catalyzing the final step of glycolysis, converting phosphoenolpyruvate to pyruvate, producing an ATP. We observed an increase in expression of PKM1 in the KO relative to the WT (Fig. 5D and E). We also measured expression of the glucose transporter GLUT1 and saw an increased in expression in KO, relative to the WT (Fig. 5F).

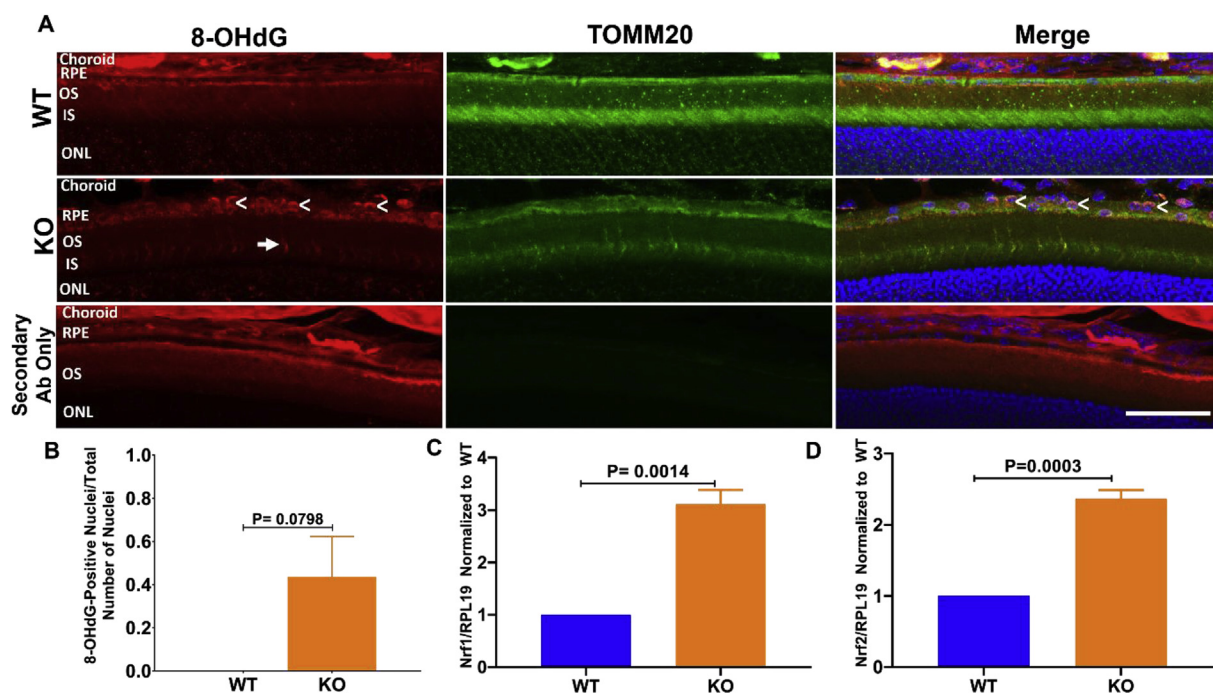


Fig. 4. Deletion of *Sod2* leads to elevated levels of oxidative stress. A) Representative IHC images with staining for 8-OHdG (red), TOMM20 (green), and DAPI (blue) from WT (top panel) and KO (middle panel) 5-month-old mice kept in normal lighting. Bottom panel shows the non-specific binding of the anti-mouse secondary antibody. < indicate examples of 8-OHdG-positive RPE cell nuclei. Arrow indicates examples of 8-OHdG-positive inner segments. White line indicates scale bar = 50 μ m. B) Quantification of percent 8-OHdG-positive RPE cells in retinal sections from A. Unpaired *t*-test, $P = 0.0798$, $n = 3$ per group, 4 images per eye. C-D) Expression of Nrf1 (C) and Nrf2 (D) mRNA in the RPE/choroid complex from 5-month-old mice kept in normal lighting. Unpaired *t*-test, $n = 3$ per group, error = SEM. Statistical significance and P-values are listed in each graph.

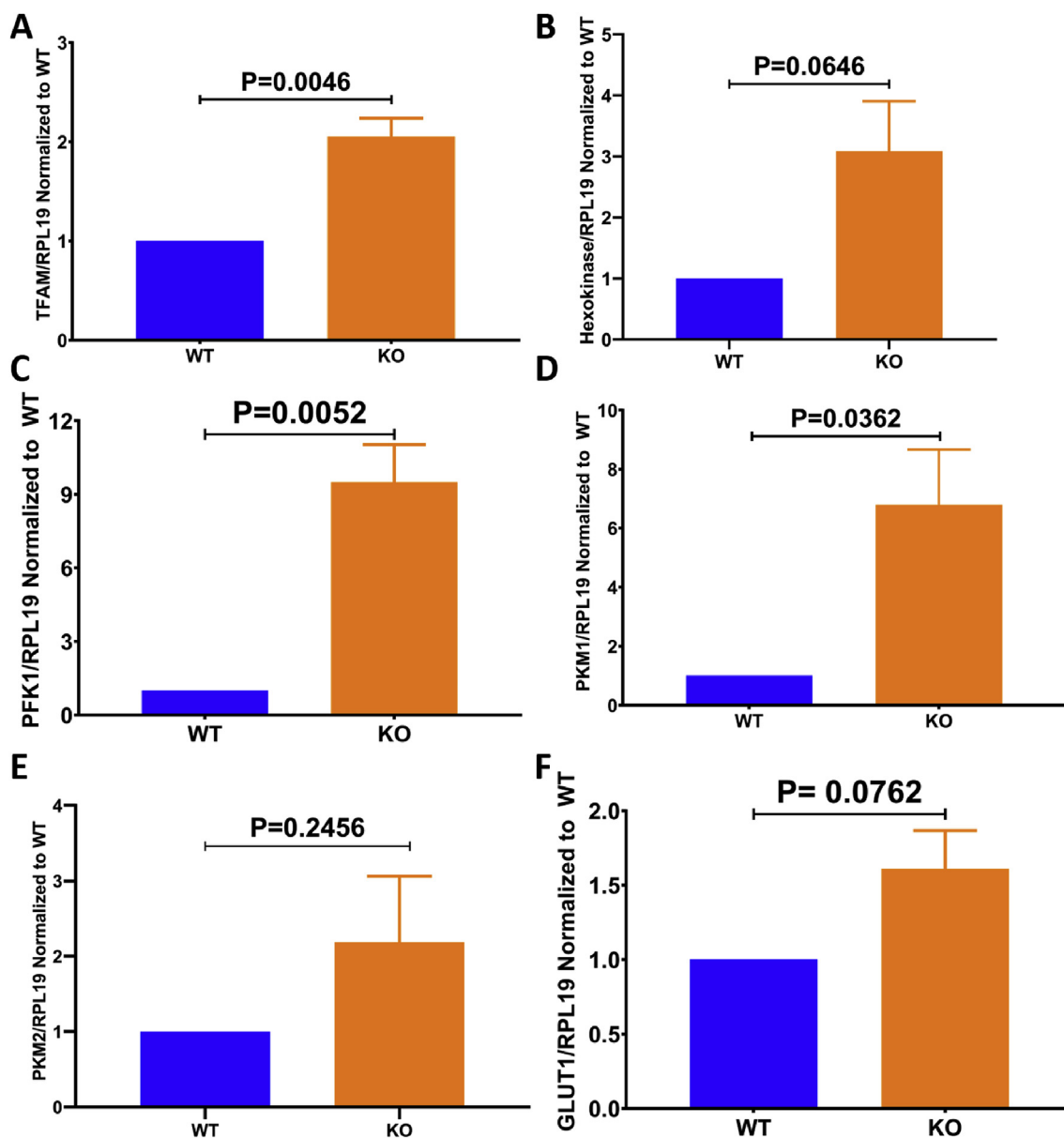


Fig. 5. Deletion of *Sod2* leads to increased levels of glycolysis-related gene expression. A-F) Gene expression levels of mitochondrial and glycolytic-related genes in the RPE/choroid complex of 5-month-old mice kept in the normal lighting normalized to RPL19 and relative to the WT. Gene expression analysis of TFAM (A), hexokinase (B), phosphofructokinase (PFK) 1 (C), PKM1 (D), PKM2 (E), and GLUT1 (F). Unpaired t-test, n = 3 per group, P-values and statistical significance are indicated above each graph, plotted error indicates SEM.

3.7. Deletion of SOD2 leads to secondary alterations in photoreceptors

Since we observed secondary effects in the photoreceptors with increased 8-OHdG staining and reduced TOMM20 staining in the inner segments of the KO as compared to the WT, we wanted to further assess potential secondary effects on the photoreceptors due to increased mitochondrial oxidative stress in the RPE, reduced RPE function, and elevated levels of gene expression of glycolytic enzymes in the RPE. Previous studies have only examined secondary loss of photoreceptor function but have not assessed any other potential secondary effects on photoreceptors. We used retinal sections and used IHC to confirm that MnSOD expression is not altered in the neuroretina. We found that expression was unaffected throughout the neuroretina in KO mice (Fig. 6A). We used EM to assess to ultra-structure of the mitochondria in the inner segments of the photoreceptors, where the mitochondria are typically most abundant in photoreceptors. We observed mitochondrial fragmentation in the mitochondria in the inner segments in the KO

mice, as compared to the WT (Fig. 6B). Since we observed mitochondrial fragmentation, we wanted to assess whether mtDNA levels may be affected. We found that there was a reduction in COXIII/ β -actin levels in the neuroretina in the KO mice as compared to the WT (Fig. 6C). We also measured ATP levels in the neuroretina, but there were no differences the WT and KO (Fig. 6D).

4. Discussion

Recent evidence suggests the importance of coordinated metabolism among the retinal cell types. Kanow et al. propose the concept of the retinal metabolic ecosystem, in which the RPE, photoreceptors, and other cell types of the retina act in concert to maintain effective metabolism in the retina [14]. Importantly, the integration of the metabolism between the photoreceptors and RPE is essential for proper function of either cell type. The RPE are responsible for transporting glucose to the photoreceptors from the choroid. The photoreceptors rely

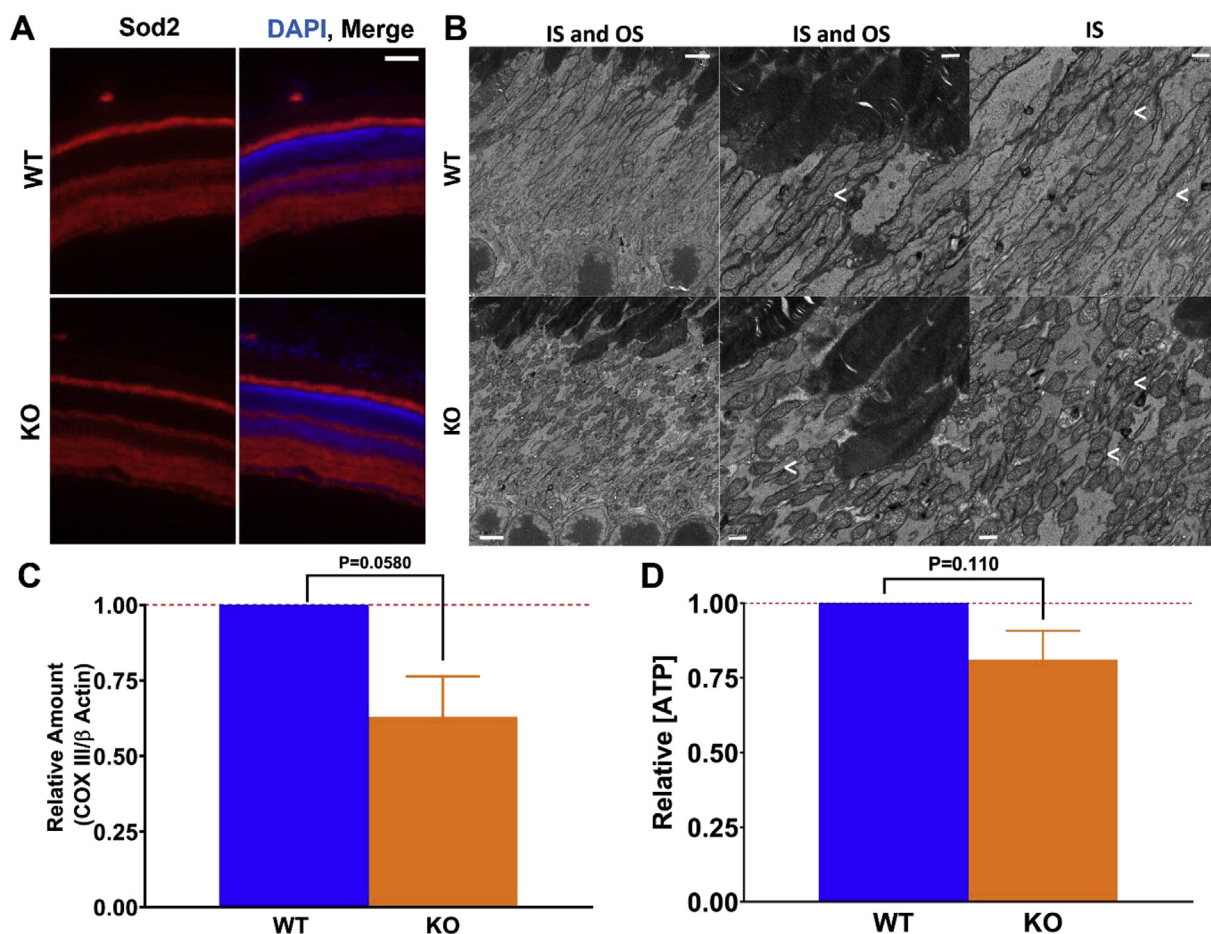


Fig. 6. Deletion of *Sod2* leads to secondary effects on photoreceptors. A) *Sod2* (red) expression in neuroretina in *Cre*-negative (WT) and *Cre*-positive (KO) animals. White line indicates scale bar = 50 μ m. B) Representative EM images from inner segments (IS) and outer segments (OS) of the photoreceptors in 5-month-old WT and KO mice kept in normal lighting. < indicate examples of mitochondria. Scale bars are indicated by white lines. For column 1 scale bar = 2 μ m. For column 2 and 3 scale bars = 0.05 μ m. C) COXIII/ β -actin levels relative to the WT in the neuroretina in 5-month-old mice kept in normal lighting. Unpaired *t*-test, $P = 0.0580$, $n = 4$ WT and 6 KO. F) ATP levels relative to the WT in 5-month-old mice kept in normal lighting. Unpaired *t*-test, $P = 0.110$, $n = 5$ WT and 6 KO. Plotted error = SEM for all graphs.

on glucose for aerobic glycolysis, which involves the production of lactate even in the presence of oxygen, a process also known as the Warburg effect, as it was discovered in tumors and in the retina by Otto Warburg in the 1920's [35,36]. Large amounts of lactate are produced by the photoreceptors, and this lactate is then transported to the RPE to be utilized for energy production. It is hypothesized that lactate serves as the signal to prevent the RPE from utilizing glucose itself, allowing glucose to remain available for the photoreceptors [14]. In addition to glycolysis, photoreceptors also rely on mitochondria for proper visual function and structure, as knockout of the mitochondrial pyruvate carrier (MPC), which is responsible for transporting pyruvate into the mitochondria to be utilized for oxidative phosphorylation, leads to loss of retinal function and disruption of retinal structure [37].

Increased oxidative stress and mitochondrial DNA lesions in the RPE may disrupt mitochondrial function and membrane potential in mitochondria in the RPE. This may lead to an energy crisis in the RPE, which could disrupt the balance of the metabolic ecosystem. Consistent with this hypothesis, several studies have suggested that AMD pathology may result from an energy crisis in the RPE [5,6,38,39]. An interesting phenomenon in AMD is that the RPE cells exhibit elevated levels of oxidative stress and dysfunctional mitochondria, but it is the parafoveal rods that are the first cells lost [40,41]. The metabolic ecosystem model predicts that a glycolytic shift in RPE could cause secondary photoreceptor loss due to lack of available glucose or other substrates and may explain this phenomenon. Consistent with the

metabolic ecosystem hypothesis, a recent study reports that loss of GLUT1 in the RPE results in reduced glucose transport through the RPE to the photoreceptors, resulting in photoreceptor starvation and degeneration [42]. Other evidence suggests that preserving the metabolic ecosystem, including enhancing glucose uptake and metabolism in photoreceptors, prevents retinal degeneration in several mouse models of inherited or induced degeneration [22,43–45], further supporting this hypothesis.

In the current study, we have demonstrated that elevated mitochondrial oxidative stress due to deletion of *Sod2* in the RPE *in vivo* is sufficient to cause RPE loss of function, which is associated with mitochondrial alterations and decreased levels of ATP. We observed an increase in gene expression of several key glycolytic enzymes in the RPE of *Sod2* KO mice, suggesting that glycolysis may be enhanced with *Sod2* KO as a compensatory mechanism for reduced mitochondrial function.

Although we did not detect a significant reduction in photoreceptor function in our study, photoreceptor impairment may take longer than 5 months, the time at which we collected retinas. In C57BL/6J mice, reduction in ERG a-wave amplitude, which arises from photoreceptors, was not observed until 6 months of age [15]. However, in this study, we did observe secondary alterations to the photoreceptors by 5 months of age, including enhanced 8-OHdG staining in the photoreceptor inner segments, reduced TOMM20 staining, fragmentation of mitochondria, and reduced COXIII/ β -actin levels. These findings are consistent with the hypothesis that the retina functions as a metabolic ecosystem with

highly coordinated metabolism between the photoreceptors and the RPE, as enhanced glycolysis and oxidative stress in the RPE may have a secondary effect on photoreceptors.

Future work involves further assessment of secondary effects on the photoreceptors with loss of *Sod2* in the RPE with aging including further investigation of how the metabolome is affected. This may involve metabolic studies that examine steady state metabolite levels and glucose labeling to determine how metabolic flux is altered in the RPE and neuroretina in this model. Further characterization of how oxidative stress products from the mitochondria may be transported to other RPE cells and to photoreceptors should be further investigated to develop a better understanding of the role of oxidative stress in this model. This study is consistent with the hypothesis that the retina functions as a metabolic ecosystem and suggests that disruptions in the metabolic interactions between the photoreceptors and RPE may be an important factor in pathogenesis of AMD.

Grant information

Research reported in this publication was supported by the National Center for Advancing Translational Sciences of the National Institutes of Health under Award Number UL1TR001427, R01 EY026268 and R01 EY016459. The content is solely the responsibility of the authors and does not necessarily represent the official views of the National Institutes of Health. Additional funding comes from the Foundation Fighting Blindness and an unrestricted grant from Research to Prevent Blindness. These funding organizations had no role in the design or conduct of this research.

Declarations of interest

None.

Acknowledgements

The authors wish to acknowledge their funding sources, including the National Center for Advancing Translational Sciences of the National Institutes of Health UL1TR001427, the National Institutes of Health R01 EY026268 and R01 EY016459, the Foundation Fighting Blindness, and an unrestricted grant from Research to Prevent Blindness. The authors also wish to acknowledge the contributions of Tara Kennell, Himani Gubbi, Raela Ridley, and Caroline Wright for their assistance in genotyping, qRT-PCR, and measuring ONL thicknesses. The authors wish to acknowledge the staff at the Robert P. Apkarian Integrated Electron Microscopy Core at Emory University for their assistance with the electron microscopy.

Appendix A. Supplementary data

Supplementary data to this article can be found online at <https://doi.org/10.1016/j.redox.2019.101201>.

References

1. P. Theurey, N.M.C. Connolly, I. Fortunati, et al., Systems biology identifies preserved integrity but impaired metabolism of mitochondria due to a glycolytic defect in Alzheimer's disease neurons, *Aging Cell* (2019) e12924, <https://doi.org/10.1111/ace1.12924>.
2. J. Tang, A. Oliveros, M.H. Jang, Dysfunctional mitochondrial bioenergetics and synaptic degeneration in alzheimer disease, *Int. NeuroUrol. J.* 23 (Suppl 1) (2019) S5–S10, <https://doi.org/10.5213/inj.1938036.018>.
3. L.F. Burbulla, P. Song, J.R. Mazzulli, et al., Dopamine oxidation mediates mitochondrial and lysosomal dysfunction in Parkinson's disease, *Science* 357 (6357) (2017) 1255–1261, <https://doi.org/10.1126/science.aam9080>.
4. M.P. Giannoccaro, C. La Morgia, G. Rizzo, V. Carelli, Mitochondrial DNA and primary mitochondrial dysfunction in Parkinson's disease, *Mov. Disord.* 32 (3) (2017) 346–363, <https://doi.org/10.1002/mds.26966>.
5. M.R. Terluk, R.J. Kapphahn, L.M. Soukup, et al., Investigating mitochondria as a target for treating age-related macular degeneration, *J. Neurosci.* 35 (18) (2015) 7304–7311, <https://doi.org/10.1523/JNEUROSCI.0190-15.2015>.
6. P.P. Karunadharm, C.L. Nordgaard, T.W. Olsen, D.A. Ferrington, Mitochondrial DNA damage as a potential mechanism for age-related macular degeneration, *Investig. Ophthalmol. Vis. Sci.* 51 (11) (2010) 5470–5479, <https://doi.org/10.1167/iovs.10-5429>.
7. W.L. Wong, X. Su, X. Li, et al., Global prevalence of age-related macular degeneration and disease burden projection for 2020 and 2040: a systematic review and meta-analysis, *Lancet Glob. Health* 2 (2) (2014) e106–e116, [https://doi.org/10.1016/S2214-109X\(13\)70145-1](https://doi.org/10.1016/S2214-109X(13)70145-1).
8. J.Y. Lim, S.Y. Lee, J.G. Kim, J.Y. Lee, H. Chung, Y.H. Yoon, Intravitreal bevacizumab alone versus in combination with photodynamic therapy for the treatment of neovascular maculopathy in patients aged 50 years or older: 1-year results of a prospective clinical study, *Acta Ophthalmol.* 90 (1) (2012) 61–67, <https://doi.org/10.1111/j.1755-3768.2009.01841.x>.
9. F. Malgorzata, Effectivity and safety of bevacizumab intravitreal injections for exudative age-related macular degeneration treatment—6 months observations, *Klin. Oczna.* 112 (7–9) (2010) 213–216.
10. G.S. Ying, J. Huang, M.G. Maguire, et al., Baseline predictors for one-year visual outcomes with ranibizumab or bevacizumab for neovascular age-related macular degeneration, *Ophthalmology* 120 (1) (2013) 122–129, <https://doi.org/10.1016/j.optha.2012.07.042>.
11. I. Bhatta, G. Luttu, Understanding age-related macular degeneration (AMD): relationships between the photoreceptor/retinal pigment epithelium/Bruch's membrane/choriocapillaris complex, *Mol. Aspect. Med.* 33 (4) (2012) 295–317, <https://doi.org/10.1016/j.mam.2012.04.005>.
12. E. Bianchi, F. Scarinci, G. Ripandelli, et al., Retinal pigment epithelium, age-related macular degeneration and neurotrophic keratouveitis, *Int. J. Mol. Med.* 31 (1) (2013) 232–242, <https://doi.org/10.3892/ijmm.2012.1164>.
13. N. Golestaneh, Y. Chu, S.K. Cheng, H. Cao, E. Poliakov, D.M. Berinstein, Repressed SIRT1/PGC-1 alpha pathway and mitochondrial disintegration in iPSC-derived RPE disease model of age-related macular degeneration, *J. Transl. Med.* 14 (1) (2016), <https://doi.org/10.1186/s12967-016-1101-8> 344-016-1101-8.
14. M.A. Kanow, M.M. Giarmarco, C.S. Jankowski, et al., Biochemical adaptations of the retina and retinal pigment epithelium support a metabolic ecosystem in the vertebrate eye, *Elife* 6 (2017), <https://doi.org/10.7554/eLife.28899>.
15. H. Mao, S.J. Seo, M.R. Biswal, et al., Mitochondrial oxidative stress in the retinal pigment epithelium leads to localized retinal degeneration, *Investig. Ophthalmol. Vis. Sci.* 55 (7) (2014) 4613–4627, <https://doi.org/10.1167/iovs.14-14633>.
16. Y.Z. Le, W. Zheng, P.C. Rao, et al., Inducible expression of cre recombinase in the retinal pigmented epithelium, *Investig. Ophthalmol. Vis. Sci.* 49 (3) (2008) 1248–1253, <https://doi.org/10.1167/iovs.07-1105>.
17. M. Strassburger, W. Bloch, S. Sulyok, et al., Heterozygous deficiency of manganese superoxide dismutase results in severe lipid peroxidation and spontaneous apoptosis in murine myocardium in vivo, *Free Radic. Biol. Med.* 38 (11) (2005) 1458–1470 S0891-5849(05)00062-6.
18. J.A. Ronchi, T.R. Figueira, F.G. Ravagnani, H.C. Oliveira, A.E. Vercesi, R.F. Castilho, A spontaneous mutation in the nicotinamide nucleotide transhydrogenase gene of C57BL/6J mice results in mitochondrial redox abnormalities, *Free Radic. Biol. Med.* 63 (2013) 446–456, <https://doi.org/10.1016/j.freeradbiomed.2013.05.049>.
19. B. Chang, N.L. Hawes, M.T. Pardue, et al., Two mouse retinal degenerations caused by missense mutations in the beta-subunit of rod cGMP phosphodiesterase gene, *Vis. Res.* 47 (5) (2007) 624–633 S0042-6989(06)00554-2 [pii].
20. M.J. Mattapallil, E.F. Wawrousek, C.C. Chan, et al., The Rd8 mutation of the *Crb1* gene is present in vendor lines of C57BL/6N mice and embryonic stem cells, and confounds ocular induced mutant phenotypes, *Investig. Ophthalmol. Vis. Sci.* 53 (6) (2012) 2921–2927, <https://doi.org/10.1167/iovs.12-9662>.
21. A. Wenzel, C.E. Reme, T.P. Williams, F. Hafezi, C. Grimm, The Rpe65 Leu450Met variation increases retinal resistance against light-induced degeneration by slowing rhodopsin regeneration, *J. Neurosci.* 21 (1) (2001) 53–58 21/1/53 [pii].
22. L. Xu, L. Kong, J. Wang, J.D. Ash, Stimulation of AMPK prevents degeneration of photoreceptors and the retinal pigment epithelium, *Proc. Natl. Acad. Sci. U. S. A.* 115 (41) (2018) 10475–10480, <https://doi.org/10.1073/pnas.1802724115>.
23. R.J. Casson, J.P. Wood, G. Han, T. Kittipassorn, D.J. Peet, G. Chidlow, M-Type pyruvate kinase isoforms and lactate dehydrogenase a in the mammalian retina: metabolic implications, *Investig. Ophthalmol. Vis. Sci.* 57 (1) (2016) 66–80, <https://doi.org/10.1167/iovs.15-17962>.
24. A. Malhotra, A. Dey, N. Prasad, A.M. Kenney, Sonic hedgehog signaling drives mitochondrial fragmentation by suppressing mitochondrial fusions in cerebellar granule neuron precursors and medulloblastoma, *Mol. Cancer Res.* 14 (1) (2016) 114–124, <https://doi.org/10.1158/1541-7786.MCR-15-0278>.
25. C.A. Schneider, W.S. Rasband, K.W. Eliceiri, NIH Image to ImageJ: 25 years of image analysis, *Nat. Methods* 9 (7) (2012) 671–675.
26. A.A. Toye, J.D. Lippiat, P. Proks, et al., A genetic and physiological study of impaired glucose homeostasis control in C57BL/6J mice, *Diabetologia* 48 (4) (2005) 675–686, <https://doi.org/10.1007/s00125-005-1680-z>.
27. A.G. Nickel, A. von Hardenberg, M. Hohl, et al., Reversal of mitochondrial transhydrogenase causes oxidative stress in heart failure, *Cell Metabol.* 22 (3) (2015) 472–484, <https://doi.org/10.1016/j.cmet.2015.07.008>.
28. T.T. Huang, M. Naeemuddin, S. Elchuri, et al., Genetic modifiers of the phenotype of mice deficient in mitochondrial superoxide dismutase, *Hum. Mol. Genet.* 15 (7) (2006) 1187–1194 dd034 [pii].
29. A. Kim, C.H. Chen, P. Ursell, T.T. Huang, Genetic modifier of mitochondrial superoxide dismutase-deficient mice delays heart failure and prolongs survival, *Mamm. Genome* 21 (11–12) (2010) 534–542, <https://doi.org/10.1007/s00335-010-9299-x>.

- [30] E. Maranzana, G. Barbero, A.I. Falasca, G. Lenaz, M.L. Genova, Mitochondrial respiratory supercomplex association limits production of reactive oxygen species from complex I, *Antioxidants Redox Signal.* 19 (13) (2013) 1469–1480, <https://doi.org/10.1089/ars.2012.4845>.
- [31] E. Lapuente-Brun, R. Moreno-Loshuertos, R. Acin-Perez, et al., Supercomplex assembly determines electron flux in the mitochondrial electron transport chain, *Science* 340 (6140) (2013) 1567–1570, <https://doi.org/10.1126/science.1230381>.
- [32] L.H. Pinto, B. Invergo, K. Shimomura, J.S. Takahashi, J.B. Troy, Interpretation of the mouse electroretinogram, *Doc. Ophthalmol.* 115 (3) (2007) 127–136, <https://doi.org/10.1007/s10633-007-9064-y>.
- [33] A. Picca, F. Fracasso, V. Pesce, et al., Age- and calorie restriction-related changes in rat brain mitochondrial DNA and TFAM binding, *Age (Dordr)*. 35 (5) (2013) 1607–1620, <https://doi.org/10.1007/s11357-012-9465-z>.
- [34] A.M. Joseph, A.A. Rungi, B.H. Robinson, D.A. Hood, Compensatory responses of protein import and transcription factor expression in mitochondrial DNA defects, *Am. J. Physiol. Cell Physiol.* 286 (4) (2004) C867–C875, <https://doi.org/10.1152/ajpcell.00191.2003>.
- [35] O. Warburg, K. Posener, E. Negelein, On the metabolism of carcinoma cells, *Biochem. Z.* 152 (1924) 309–344.
- [36] O. Warburg, F. Wind, E. Negelein, The metabolism of tumors in the body, *J. Gen. Physiol.* 8 (6) (1927) 519–530.
- [37] A. Grenell, Y. Wang, M. Yam, et al., Loss of MPC1 reprograms retinal metabolism to impair visual function, *Proc. Natl. Acad. Sci. U. S. A.* 116 (9) (2019) 3530–3535, <https://doi.org/10.1073/pnas.1812941116>.
- [38] D.A. Ferrington, M.C. Ebeling, R.J. Kapphahn, et al., Altered bioenergetics and enhanced resistance to oxidative stress in human retinal pigment epithelial cells from donors with age-related macular degeneration, *Redox Biol.* 13 (2017) 255–265 S2213-2317(17)30287-2 [pii].
- [39] D.A. Ferrington, R.J. Kapphahn, M.M. Leary, et al., Increased retinal mtDNA damage in the CFH variant associated with age-related macular degeneration, *Exp. Eye Res.* 145 (2016) 269–277 S0014-4835(16)30017-3 [pii].
- [40] C. Owsley, G.R. Jackson, A.V. Cideciyan, et al., Psychophysical evidence for rod vulnerability in age-related macular degeneration, *Investig. Ophthalmol. Vis. Sci.* 41 (1) (2000) 267–273.
- [41] C.A. Curcio, N.E. Medeiros, C.L. Millican, Photoreceptor loss in age-related macular degeneration, *Investig. Ophthalmol. Vis. Sci.* 37 (7) (1996) 1236–1249.
- [42] A. Swarup, I.S. Samuels, B.A. Bell, et al., Modulating GLUT1 expression in retinal pigment epithelium decreases glucose levels in the retina: impact on photoreceptors and Muller glial cells, *Am. J. Physiol. Cell Physiol.* 316 (1) (2019) C121–C133, <https://doi.org/10.1152/ajpcell.00410.2018>.
- [43] L. Zhang, J. Du, S. Justus, et al., Reprogramming metabolism by targeting sirtuin 6 attenuates retinal degeneration, *J. Clin. Investig.* 126 (12) (2016) 4659–4673 86905 [pii].
- [44] N. Ait-Ali, R. Fridlich, G. Millet-Puel, et al., Rod-derived cone viability factor promotes cone survival by stimulating aerobic glycolysis, *Cell* 161 (4) (2015) 817–832, <https://doi.org/10.1016/j.cell.2015.03.023>.
- [45] A. Venkatesh, S. Ma, Y.Z. Le, M.N. Hall, M.A. Ruegg, C. Punzo, Activated mTORC1 promotes long-term cone survival in retinitis pigmentosa mice, *J. Clin. Investig.* 125 (4) (2015) 1446–1458, <https://doi.org/10.1172/JCI79766>.